APL Materials

RESEARCH ARTICLE | MAY 07 2021

Tuning electronic properties of conductive 2D layered metal–organic frameworks via host–guest interactions: Dioxygen as an electroactive chemical stimuli

Special Collection: 2D Materials Chemistry

Mohammad R. Momeni ; Zeyu Zhang; David Dell'Angelo; Farnaz A. Shakib

APL Mater. 9, 051109 (2021)
https://doi.org/10.1063/5.0049317

Tuning electronic properties of conductive 2D layered metal–organic frameworks via host–guest interactions: Dioxygen as an electroactive chemical stimuli

Cite as: APL Mater. 9, 051109 (2021); doi: 10.1063/5.0049317
Submitted: 3 March 2021 • Accepted: 18 April 2021 •
Published Online: 7 May 2021

Mohammad R. Momeni,[a),b)] Zeyu Zhang,[b)] David Dell'Angelo,[b)] and Farnaz A. Shakib[b),c)]

AFFILIATIONS

Department of Chemistry and Environmental Science, New Jersey Institute of Technology, Newark, New Jersey 07102, USA

Note: This paper is part of the Special Topic on 2D Materials Chemistry.
[a)]**Electronic mail:** momeni@njit.edu
[b)]**URL:** https://research.njit.edu/mdmsl/
[c)]**Author to whom correspondence should be addressed:** shakib@njit.edu

ABSTRACT

Thermodynamics and kinetics of O_2 adsorption and its impacts on structural features and conductive behavior of 2D π-stacked layered metal–organic frameworks (MOFs) are studied using periodic PBE-D3 quantum mechanical calculations. Our computed O_2 adsorption energies of $Co_3(HTTP)_2$ (HTTP = hexathiotriphenylene), as a representative of the 2D MOFs family, show that not only open-Co(II) sites but also redox-active HTTP linkers take part in chemisorption of O_2 by forming strong S=O bonds. This is in contrast to conventional 3D $Co_2(OH)_2(BBTA)$ and $Fe_2(dobdc)$ MOFs with similar hexagonal 1D channels where O_2 adsorption occurs solely via coordination to the open-metal sites. Due to the adsorptive capability of its redox-active linkers, $Co_3(HTTP)_2$ is superior to the analogues 3D MOFs where the change in the oxidation state of the transition metal centers is suggested to result in hindering both the kinetics and thermodynamics of the adsorption process. Our calculated band structures and density of states show that the conductive behavior of the studied $Co_3(HTTP)_2$ 2D MOF changes dramatically from metallic in the parent system to semiconducting under oxygen rich conditions, with direct bandgap openings that range from 123 to 251 meV. The results presented in this work are helpful in understanding the effects of different electroactive guest molecules on the structure and conductive behavior of 2D layered MOFs and related nonporous materials.

I. INTRODUCTION

Metal–organic frameworks (MOFs) are a promising class of porous hybrid organic/inorganic materials with a wide variety of applications in energy storage and conversion,[1–3] catalysis,[4–6] carbon capture and sequestrations,[7–9] as well as water harvesting and purification.[10–12] Combining the exceptional thermal, chemical, and mechanical stability of MOFs with their tunable chemical environments allows selective uptake and retention/storage of gas molecules, turning them into excellent materials for adsorption, storage, and controlled release of different adsorbates under a variety of operating conditions.[13,14] MOFs with open-metal sites are specifically suited for adsorptive separation of different gaseous mixtures depending on the strength of the coordinative bonds formed between the adsorbate molecules and the open-metal sites.[13,14] Among different adsorbates, studying O_2 adsorption as an electroactive chemical stimulus is of an utmost importance as traces of oxygen can alter the crystal morphology of the studied material and its electrical properties significantly. As a notable example, Dou *et al.* have recently shown that the presence of O_2 is necessary for the synthesis of microcrystalline 2D electrically conductive $M_3(HIB)_2$, HIB = hexaiminobenzene and M = Ni and Cu, while in the absence of air, only amorphous gray powders would form instead.[15] Shen *et al.* showed that one can fine-tune layer stacking

patterns and linker conformations of 2D ZUL-100 and ZUL-200 MOFs through linker oxidation in order to achieve selective adsorptive separation of ethylene from acetylene.[16] Selective adsorption of O_2 is also known to be beneficial in tuning the electronic properties of different materials for further separation of other strategic gaseous mixtures. Very recently, Li and co-workers have introduced O_2 chemisorption in the Fe_2(dobdc) (dobdc^{4-} = 2,5-dioxido-1,4-benzenedicarboxylate) 3D MOF[17] with open-iron(II) sites as a new strategy for selective separation of ethane from ethylene with 99.99% efficiency [Fig. 1(a)].[18] Through neutron diffraction analysis and theoretical calculations, it was subsequently shown that chemisorption of molecular oxygen by the open-iron(II) sites leads to the formation of iron(III)–peroxo sites that preferentially bind to ethane over ethylene.[18] This demonstrates that MOFs with high O_2 uptakes are promising candidates for creating an extremely efficient platform for the adsorptive separation of different gaseous mixtures.

In addition to open-metal sites, recent experimental studies have explored the role of organic linkers on O_2 adsorption as well. Long and co-workers have revealed that one can significantly boost the O_2 adsorption capacity of the $Co_2(Cl)_2$(BBTA) [H_2BBTA = 1H,5H-benzo(1,2-*d*),(4,5-*d*′)bistriazole] 3D MOF by replacing its μ_2-Cl groups with μ_2-OH in $Co_2(OH)_2$(BBTA) [Fig. 1(b)].[19] Subsequent theoretical studies attributed the high O_2 uptake in $Co_2(OH)_2$(BBTA) to the ability of the μ_2-OH groups to form hydrogen bonds (HBs) with the newly formed Co–O_2 coordinative bonds and thereby stabilize them.[19,20] Nevertheless, an overall slow kinetic was observed for chemisorption of O_2, which was attributed to a change in the oxidation state of the open-Co sites from +2 to +3 upon binding to the electroactive oxygen molecules, hindering the overall efficiency of this material.[19]

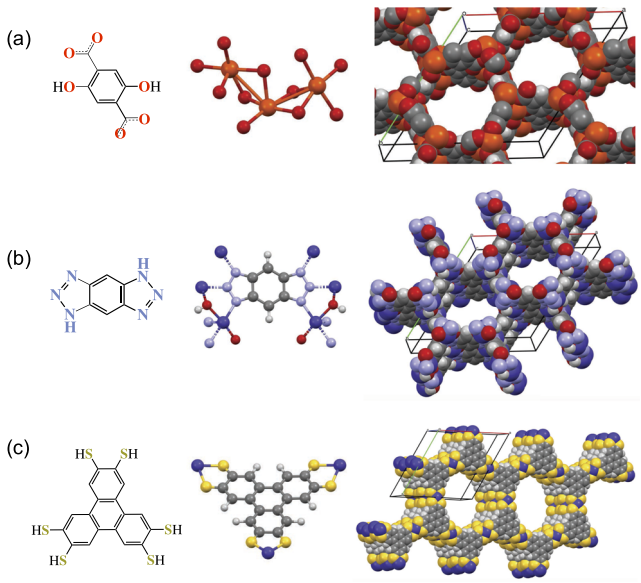

FIG. 1. Crystal structures of 3D (a) Fe_2(dobdc) (dobdc^{4-} = 2,5-dioxido-1,4-benzenedicarboxylate), (b) $Co_2(OH)_2$(BBTA) [H_2BBTA = 1H,5H-benzo(1,2-*d*),(4,5-*d*′)bistriazole], and (c) 2D π-stacked layered Co_3(HTTP)$_2$ (HTTP = 2,3,6,7,10,11-hexathiotriphenylene) MOFs along their main hexagonal 1D channels. The hexagonal unit cells are shown as black lines. Gray = C, white = H, light blue = N, red = O, yellow = S, orange = Fe, and dark blue = Co.

Recently introduced 2D layered conductive MOFs [Fig. 1(c)],[21–25] which contain open-metal sites along with redox-active organic linkers, are unique materials for selective adsorption of electroactive molecules such as O_2 from both thermodynamic and kinetic points of view. The infinite hexagonal 1D mesoporous channels (~2 nm) along the stacking direction allow different target adsorbates to freely enter the pores and interact with both open-metal sites and redox-active linkers. In a recent study, we have demonstrated the active role of organic linkers of the Co_3(HTTP)$_2$ (HTTP = hexathiotriphenylene) 2D MOF in oxidative dehydrogenation of propane via adsorbing the oxygen atom from the N_2O oxidizing agent.[26] On the other hand, O_2 adsorption can potentially open up unprecedented opportunities for tuning the intrinsic electrical conductivity of 2D MOFs via host–guest interactions. Experimentally, it is not straightforward to disentangle the mechanism of O_2 adsorption (i.e., via coordination to the open-metal sites and/or organic linkers) and its impacts on the structure and electronic properties of the material at the molecular level. Here, we take up this challenge by means of accurate periodic quantum mechanical calculations. We compare the O_2 adsorption capability of the Co_3(HTTP)$_2$ 2D MOF to those of 3D $Co_2(OH)_2$(BBTA) and Fe_2(dobdc) materials, all of which have infinite 1D hexagonal channels along their stacking directions (see Fig. 1). The main geometrical difference is that in 3D $Co_2(OH)_2$(BBTA) and Fe_2(dobdc) MOFs, layers are covalently bonded, while in the considered 2D Co_3(HTTP)$_2$ system, layers are connected via rather weaker van der Waals interactions. We will show how this feature increases the adsorptive capacity of 2D MOFs, which, in turn, changes their structural features drastically. Subsequently, we explore how these profound changes alter the conductive nature of Co_3(HTTP)$_2$. Previously, we have characterized three different classes of dynamical motions in 2D MOFs,[26–28] and our unpublished results show their effective role in determining the conductive behavior of these systems. However, to be able to compare the intrinsic adsorption capabilities of 2D MOFs vs 3D MOFs on equal footing, specially determining the roles of redox active transition metal sites and organic linkers, we did not consider the dynamic motions of the former materials in this work. We believe that the results presented in this work are helpful in paving the way for future studies on disentangling the effects of different 2D vs 3D MOF morphologies on adsorption of small electroactive adsorbate molecules and their subsequent impacts on the conductive behavior of the studied materials.

II. COMPUTATIONAL METHODS

A. Periodic electronic structure calculations

The crystal structure of the Co_3(HTTP)$_2$ (HTTP = hexathiotriphenylene) MOF was taken from our previous study,[26] while the crystal structures of $Co_2(OH)_2$(BBTA)[29] and Fe_2(dobdc)[17] MOFs were obtained from the experiment. Both atomic positions and cell vectors of all parent and oxygenated systems were minimized; XYZ coordinates of all crystal structures are provided as part of the supplementary material. Periodic boundary conditions as

implemented in the quickstep module of CP2K version 7.1[30] were used. Spin-polarized PBE[31] with damped D3 dispersion correction[32] and double-zeta valence with polarization DZVP-MOLOPT basis sets and core-electron pseudopotentials according to the Goedecker–Teter–Hutter formulation[33] were performed. A recent benchmark study[34] has shown that the employed methodology in this work yields adsorption energies that are close to those of PBE-D3+U and meta-generalized gradient approximation (meta-GGA) M06-L data. Furthermore, it is shown that in the case of the layered $(NiC_4S_4)_3$ 2D MOF, the D3 dispersion correction is able to capture the weak van der Waals interactions by predicting the correct stacking order, reduced inter-layer distances, and vertical corrugation.[35] The plane-wave cutoff of the finest grid and REL_CUTOFF were set to 500 and 60 RY. The MAX_FORCE (hartree/bohr), RMS_FORCE, MAX_DR (bohr), and RMS_DR were set to 0.0030, 0.0050, 0.0020, and 0.0050, respectively.

B. Cluster electronic structure calculations

Cluster models were cut from the corresponding periodic optimized dry $Co_3(HTTP)_2$ models. The triphenylene linkers were truncated at the catecholates with the position of the end carbon atoms kept frozen to represent the rigidity of the MOF. The end carbon atoms of the formed catecholate linkers were then caped with hydrogen, resulting in a neutral cluster. Singlet, triplet, and quintet spin states were considered for all studied systems, where in agreement with previous studies,[36–38] a high spin quintet state was found to be the most stable isomer on the potential energy surfaces of all studied species. Geometry optimizations were then performed in the gas phase using the local meta-GGA M06-L[39] density functional and the def2-SVP[40,41] basis set for all elements. The nature of all stationary points was determined by the calculation of analytical vibrational frequencies, which were also used to compute molecular partition functions (300 K, 1 atm) using the conventional particle-in-a-box, rigid-rotator, quantum mechanical harmonic oscillator approximation,[42] except that all vibrational frequencies below 50 cm^{-1} were replaced with a value of 50 cm^{-1} (the quasi-harmonic-oscillator approximation).[42] Zero-point vibrational energies and thermal contributions to enthalpy were determined from these partition functions. For transition-state structures, the presence of a single imaginary frequency corresponding to the reaction path of interest was confirmed. The electronic energies were further refined by performing single-point energy calculations at the M06-2X[43,44] meta-GGA hybrid density functional on the M06-L optimized geometries using the larger def2-TZVP[40,41] basis set. Default convergence criteria for geometry optimizations and single point energy calculations were used. All reported enthalpies (300 K, 1 atm) are computed by combining M06-2X single point energies with thermochemical contributions obtained at the M06-L level. All cluster computations were carried out using Gaussian 16 version A.03.[45]

C. Electronic band structure calculations

The band structure (BS) and density of states were calculated at the PBE[31] level corrected by the D3 method of Grimme[32] as implemented in the Vienna *Ab Initio* Simulation Package (VASP).[46–49] Hubbard U corrections were included to treat 3d states of the Co transition metals.[50–52] Here, only the difference between Coulomb term U and exchange term J, defined as U_{eff} = U - J, was taken into consideration with the value of U_{eff} set to 5.3 eV for Co as suggested by Mann *et al.*[53] Interactions between electrons and ions were described by Projector Augmented Wave (PAW) potentials[54,55] with the energy cutoff set to 500 eV. Gaussian smearing was adopted in all calculations with a smearing width of 0.05 eV. The convergence criteria were 10^{-5} for self-consistent field calculations and 10^{-6} for electronic property calculations. A *k*-point mesh in the Monkhorst–Pack scheme of 2 ×2× 6 was used in the SCF part and twice denser in the following calculations. Spin polarized calculations (collinear) were performed for all systems.

III. RESULTS AND DISCUSSIONS

A. Thermodynamics of O_2 adsorption

Using periodic quantum mechanical calculations, we first investigate the effects of different MOF morphologies and the presence of redox-active linkers on physisorption and chemisorption of dioxygen molecules (Fig. 2). Four different O_2 bound isomers were found for the 2D layered $Co_3(HTTP)_2$ MOF due to the affinity of not only open-Co sites but also thio functional groups of HTTP linkers for adsorbing oxygen (Fig. 2). This is in contrast to $Co_3(HHTP)_2$, HHTP = hexahydroxytriphenylene, with only one mode of O_2 adsorption, which is through coordination to the open-Co site (**2D-Co** in Fig. 2) with an exothermic adsorption energy (ΔE_{ads}) of −19.2 kcal/mol. The corresponding isomer in the $Co_3(HTTP)_2$ MOF is **2D-S-Co**, where the coordination of one oxygen atom of O_2 to the open-Co site is accompanied by chemisorption of the other oxygen by the thio functional group. The formation of Co=O and S=O bonds compensates for the dissociation of the O_2 bond, resulting in a ΔE_{ads} value of −36.2 kcal/mol, i.e., 17 kcal/mol more exothermic than **2D-Co**, emphasizing the effective role of the redox-active HTTP linkers on O_2 adsorption. Two more stable O_2 adducts were located on the PES of $Co_3(HTTP)_2$, i.e., **2D-S-S** and **2D-S-S(int)**, where O_2 is chemisorbed on two thio groups either in the same layer (with a ΔE_{ads} value of −46.2 kcal/mol) or in two different layers (with a ΔE_{ads} value of −49.4 kcal/mol). The relatively low computed ΔE_{ads} value for **2D-S-Co** compared to these two adducts is likely due to the change in the formal oxidation state of Co upon chemisorbing electroactive O_2 molecules. The adsorption of O_2 by the open-Co sites in $Co_3(HHTP)_2$ (**2D-Co**) is found to be 8.4 and 19.0 kcal/mol less thermodynamically favorable than the analogues 3D Fe and Co MOFs (Fig. 2). This is likely due to the lower coordination number of Co in the 2D $Co_3(HHTP)_2$ MOF compared to the 3D analogues, which makes the change in the oxidation state of the involved transition metal even more destabilizing. The rather high adsorption energy of **3D-O-Co** is also, in part, due to a stabilizing hydrogen bond (HB) formation between the Co(III)–peroxo species and the nearby bridging μ_2-hydroxyl group as has been pointed out before.[20] We also investigated the thio analogue of the 3D Co MOF [i.e., $Co_2(SH)_2(BBTA)$] to probe the impact of linker modification on the overall O_2 adsorption process. Interestingly, the redox-active nature of the $Co_2(SH)_2(BBTA)$ organic linkers allows dioxygen to be chemisorbed on the thio linkers in addition to bonding to the open-Co sites (Fig. 2). This creates direct comparisons between 2D and 3D O_2

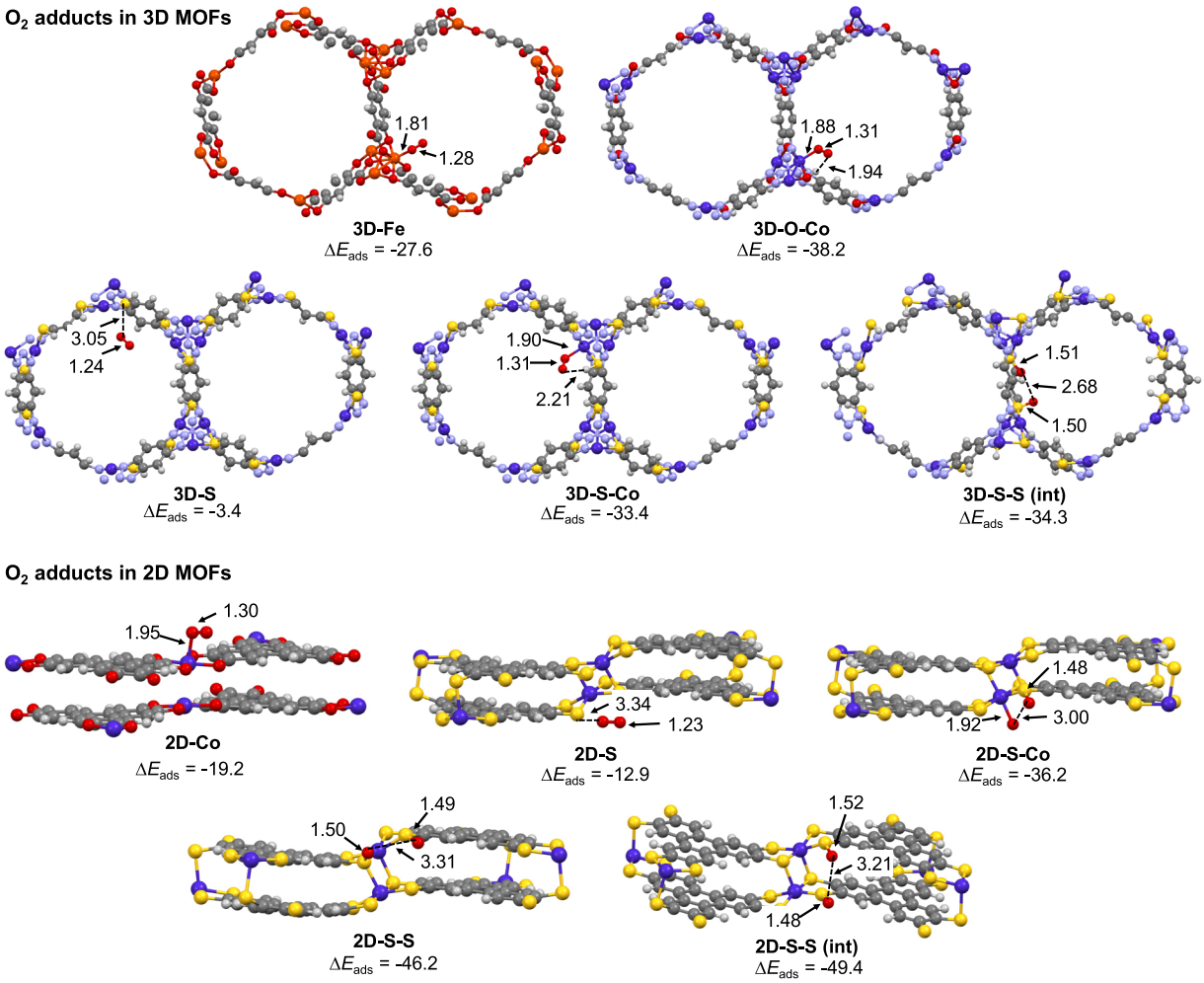

FIG. 2. Key bond distances (Å, PBE-D3) of different O_2 adducts along with their calculated adsorption energies (kcal/mol, PBE-D3) for 3D (top) and 2D layered (bottom) MOFs. Isolated species are considered as zero of energy; see Fig. 1 for color codes.

bound isomers. Among 2D isomers, the one where O_2 is physisorbed by a thio group (**2D-S**) has the lowest adsorption energy of −12.9 kcal/mol. Still, comparison between this isomer and its analogue in the 3D $Co_2(SH)_2$(BBTA) MOF (**3D-S**) shows a higher adsorption energy of 9.5 kcal/mol. Similarly, adsorption is more favored in **2D-S-Co** and **2D-S-S(int)** than in **3D-S-Co** and **3D-S-S(int)** by 2.8 and 15.1 kcal/mol, respectively. Overall, the adsorption of O_2 via redox-active linkers, which is often overlooked, can potentially lead to remarkably fast adsorption kinetics since it can occur without a change in the oxidation state of the transition metal. Finally, it should be noted that the presented data in this work are obtained at 0 K. Inclusion of temperature can potentially induce various dynamical motions in the studied 2D layered MOFs. These motions can potentially increase the variety of adsorption sites, as we have shown in our previous work,[26] and overall increase the adsorption capability of these materials.

B. Kinetics of O_2 adsorption

As shown in Sec. III A, the formation of all four O_2 bound isomers in the 2D layered Co_3(HTTP)$_2$ MOF is thermodynamically favorable. In order to verify that the formation of these stable O_2 adducts is not kinetically hindered, we cut cluster dimers from the periodic PBE-D3 optimized crystal structures with the end carbon atoms fixed and truncated to hydrogen to represent the rigidity of the MOF framework. Focusing only on the three chemisorbed adducts, we obtained the transition states (TSs) for O_2 adsorption at the M06-2X/def2-TZVP//M06-L/def2-SVP level, the results of which are depicted in Fig. 3. Many TSs with different spin states were surveyed to arrive at the complexes shown. Figure 3(a) represents the transition state of formation of **2D-S-Co**, where O_2 is being dissociated between two Co centers and the nearby thio group. Due to including zero-point vibrational energy effects, the

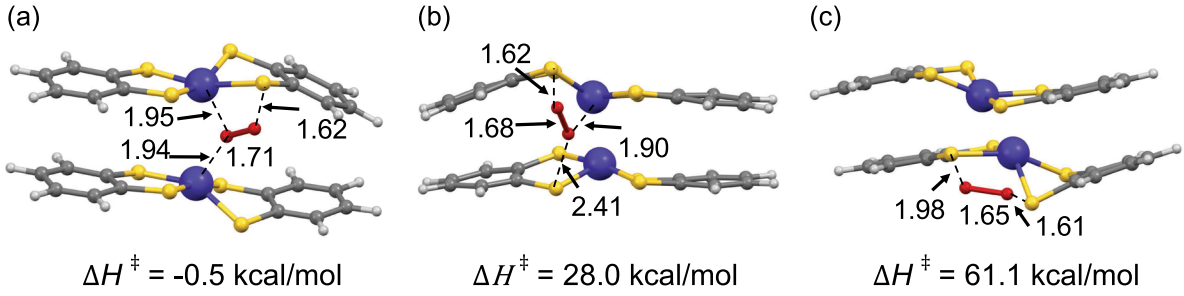

FIG. 3. Key bond distances (Å, M06-L) in transition states for chemisorption of O_2 on cluster models of 2D $Co_3(HTTP)_2$ MOF with dioxygen shared between (a) two Co, (b) one Co, and (c) no Co transition metal sites. The M06-2X//M06-L computed activation enthalpy ($\Delta H^{\ddagger}$ in kcal/mol) is given for comparison. Isolated species are considered as zero of energy; see Fig. 1 for color codes.

computed barrier is negative, which clearly hints that the O_2 splitting is barrier-less for this isomer. Figure 3(c) represents the transition state for the formation of **2D-S-S**, which involves only thio groups and no Co centers. This isomer is shown to possess the highest calculated barrier of all. The transition state for the formation of the **2D-S-S(int)** isomer corresponds to O_2 being dissociated between two thio groups and one Co center [Fig. 3(b)]. This isomer has a $\Delta H^{\ddagger}$ value of 28.0 kcal/mol, which falls in between the other two TSs. The observed trend reveals that in order for the O_2 splitting to occur, at least one Co atom needs to be involved in the process. Hence, **2D-S-S** and **2D-S-S(int)** O_2 adducts are unlikely to form at ambient conditions. On the other hand, O_2 adsorption by means of dissociation on a neighboring Co center and the thio group to form a **2D-S-Co** adduct is both thermodynamically and kinetically feasible. To summarize this section, we have shown that linker-mediated O_2 splitting in the 2D layered $Co_3(HTTP)_2$ MOF is thermodynamically and kinetically feasible. This finding is in agreement with our previous study[26] where using equilibrated structures at a finite temperature of 293 K, we showed that the adsorption of oxygen atoms in $Co_3(HTTP)_2$ is most favored on defect sites, which allows oxygen to bridge between Co and thio groups. Our detailed mechanistic study showed that this mode of adsorption has the lowest activation energy and the most negative change in Gibbs free energy among the studied catalytically active sites. It is also consistent with recent reports of efficient ligand-centered electrocatalytic oxygen reduction reactions on other members of the 2D MOF family, $Ni_3(HITP)_2$ (HITP: hexaiminotriphenylene)[56–59] and $Ni_3(HAB)_2$ (HAB = hexaaminobenzene).[60] We attribute this phenomenon to the fact that this mode of adsorption has minimal effect on the oxidation states of the open-metal sites. As a result, the thermodynamics and kinetics of the overall adsorption process are not hindered. This finding is especially important as it can potentially open new avenues when porous materials for higher and faster uptakes of electroactive adsorbates with oxidation/reduction capabilities are explored. The 2D MOFs family is known for its electrically conductive nature. In what comes next, we show how the adsorption of electroactive dioxygen molecules and their splitting can potentially alter the electronic properties of these materials.

C. Electronic properties

By construction, MOFs exhibit low electrical conductivity due to redox-inactive organic ligands that bind to hard-metal ions. The majority of reported MOFs are large bandgap insulators (i.e., electronic bandgaps >4 eV) with a few examples of metallic ones such as $Ni_3(HAB)$[15] 2D MOF or semiconducting ones such as $Zn_2(TTFTB)$, TTFTB = tetrathiafulvalene tetrabenzoate,[61] 3D MOF with a computed electronic bandgap of 1.75 eV. Oxidizing agents such as I_2 have long been used as chemical stimuli to boost the electrical conductivity of different materials via creating mixed valency states.[62–65] Here, we intend to show that O_2 can similarly be used to tune the electronic properties of 2D MOFs. We present the results of our band structure (BS) and atomic orbital projected density of state (pDOS) calculations to probe how the conductive behavior of 2D MOFs is affected after being fully oxygenated compared to the parent system. It should be noted that the adsorption of guest molecules may affect the conductive character of the system in two different ways. First, it can result in structural deformations that can affect both intra- and inter-layer charge transport pathways. Second, the guest molecules can act as charge carriers themselves. The PBE-D3 minimized structures of the oxygenated MOF compared to the parent system are given in Fig. 4.

While the parent system shows a stepped geometry of layers, the presence of oxygen atoms chemisorbed by both metal nodes and organic linkers creates more planar layers. Nevertheless, the most striking geometrical difference is an increase in the inter-layer

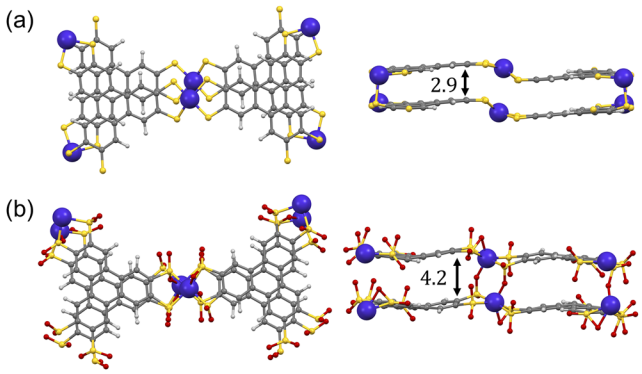

FIG. 4. Top and side views of the PBE-D3 minimized (a) parent and (b) fully oxygenated $Co_3(HTTP)_2$ systems with key interlayer distances given in Å; see Fig. 1 for color codes.

distance from 2.9 Å in the parent system to 4.2 Å in the oxygenated material in order to accommodate the incoming guest molecules. This can potentially reduce the through-space interactions between layers and affect the inter-layer conduction pathway.

The PBE+U computed BS and pDOS diagrams of both parent and oxygenated MOFs with the U parameter set to 5.3 eV, as suggested by Mann *et al.*,[53] are illustrated in Fig. 5. Their recommendation of this value for the U parameter was through linear response calculations for 3d orbitals of Co^{2+} centers in Co-MOF-74 where it yielded cell parameters that were in excellent agreement with experimental values, i.e., a = 6.92 vs 6.85 Å and c = 15.35 vs 15.13 Å. Investigation of CO_2 adsorption energy through forming the Co–O bond against different U parameters ranging from 0.0 to 5.3 eV showed no significant changes in the metal's d character. It is in fact the Co–O bond length that was shown to become slightly shorter due to the increase in the U value, from 2.82 to 2.68 Å, when the U parameter was increased from 0.0 to 5.3 eV. For comparison, the Co–O bond length of Co to the carboxylate ligand in Co-MOF-74 is ~2.06 Å. These results suggest that U = 5.3 eV is, indeed, a good choice for our systems as well. Generally, 2D MOFs are expected to have an anisotropic conductive nature. The competition between through-bond, along the 2D layers, and through-space, along the stacking direction, charge mobilities is dictated by the relative slope of the band dispersions (i.e., the derivative of the energy with respect to the crystal momentum $\frac{\partial E}{\partial k}$) and by the effective masses (i.e., the inverse of the second derivative). The parent $Co_3(HTTP)_2$ MOF shows metallic character along the stacking direction, i.e., the Γ–A region of the BS in Fig. 5(a), with bands crossing the Fermi level. This observation is consistent with the conductivity of 3.2×10^{-2} S cm^{-1} measured for $Co_3(HTTP)_2$ films with a thickness of 0.2 μm.[24] The character of the frontier orbitals is key to discern the atomic contributions to different conduction pathways. To have a clear picture of this contribution, two different pDOS diagrams are shown in Fig. 5. The top left diagrams show the contribution of orbitals that are oriented in the *ab* plane, and the top right diagrams demonstrate orbitals that are oriented along the *c* direction. We note that the first group of orbitals can only contribute to the intra-layer conduction pathway, while the second group can contribute to both intra-and inter-layer pathways due to extended π–d conjugation along the layer and π–π interactions between adjacent layers. Examining these diagrams reveals that the bands near the Fermi level are almost fully contributed by the S and C p_z orbitals of the ligand and the delocalized d_z orbitals of Co. However, the $p_{x,y}$ orbitals of sulfur also indicate a small contribution to the Fermi level, which can be the result of the stepped geometry of the layers. The conduction band (CB) minimum along the MKΓ line is found to touch the highest energy point of the valence band (VB), pointing out the potential of inducing an intra-layer semiconductive behavior by means of host–guest interactions. Alternatively, the bandgap opening can be engineered through temperature-induced dynamic motions. The situation is very similar in the LHA region; only in this case, we can already observe a slight band opening characterized by overlaps between the deep VB and CB. Indirect gaps and the valleys on each side of the bandgap point to a possible hopping

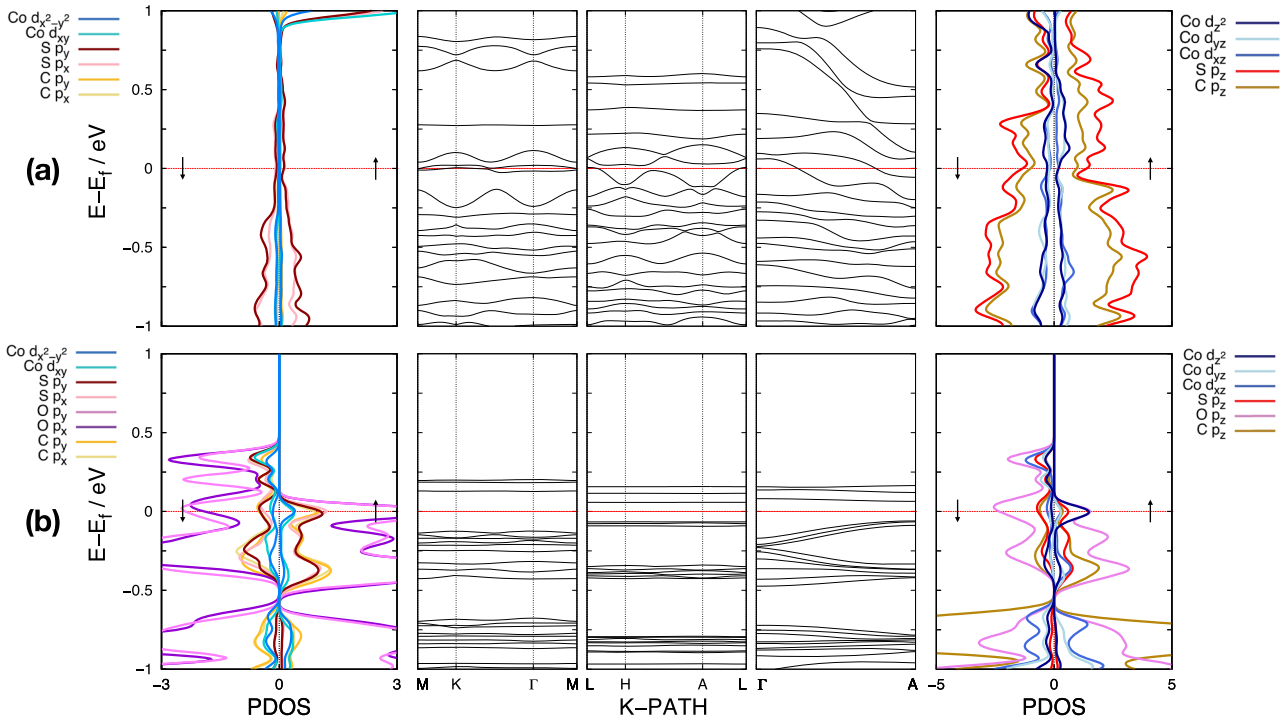

FIG. 5. PBE+U calculated band structures and projected density of states of the parent (a) and fully oxygenated (b) $Co_3(HTTP)_2$ systems. The Fermi level is highlighted with a dashed red line. The arrows ↑ and ↓ represent spin-up and spin-down, respectively.

mechanism between trap states for charge transport along the 2D layers. The BS and pDOS diagrams of the oxygenated system disclose a dramatic change in the charge mobility following the chemisorption of the O_2 guest molecules. As a consequence of the polaron states introduced by the electroactive O_2 molecules, both intra- and inter-layer bandgaps open up at the Fermi level. The conductive behavior of the MOF deviates from being anisotropic/metallic in the parent system to isotropic/semiconducting in the oxygenated one. As shown in Fig. 4, the formation of S=O and Co=O bonds creates cross-links between adjacent layers, which leads to a 44.8% expansion of the inter-layer distance compared to the parent MOF and affects through-space charge mobility in the studied 2D MOF as evident from the rather flat bands along the stacking direction, i.e., ΓA direction [Fig. 5(b)]. This finding is in agreement with previous studies,[66,67] which show that the increase in the inter-layer distance reduces the through-space charge mobility. Interestingly, very flat bands are also evident in the intra-layer direction, which implies that intra-layer electronic communication between ligands is essentially non-existent. This is the result of a deformed octahedral metal complex formed after adsorption of two oxygen atoms in axial positions, which acts as a nodal point. This can be confirmed from the frontier orbital localization on Co as evident from d_{z^2}, $d_{x^2-y^2}$, and d_{xy} peaks in the oxidized system. Figure 6 demonstrates the highest occupied crystal orbital (HOCO) of the parent and oxygenated MOFs. Calculated isosurface densities clearly show that the almost octahedral metal node in the oxygenated system does not allow electronic communications between the ligands as discussed above. Examining the frontier orbitals clearly demonstrates O *p* orbitals as the main contributors to both the VB and CB. In conclusion, the adsorption of O_2 molecules has a two-fold effect on the conductive behavior of the studied system: (i) by inducing structural deformations that can affect both intra- and inter-layer charge transport pathways and (ii) by O_2 molecules acting as charge carriers themselves.

Finally, to provide an insight into the effects of different Hubbard U corrections on the observed electronic properties, we benchmarked three different U parameters with U = 0 (i.e., PBE-D3 calculations without Hubbard U corrections), U = 4 eV (which is considered the universal value that yields reasonably accurate results for all transition metals),[69,70] and U = 5.3 eV recommended[53] for Co 3d orbitals, which we used as the parameter of choice in this work. We compiled the resulted bandgaps in Table I with the corresponding BS diagrams reported in the supplementary material (Fig. S1); for the effect of the number of *k*-points on the computed BSs, see the supplementary material (Fig. S2). It is clear that the semiconductive nature of the oxygenated MOF is not affected by the choice of U parameter. The parent $Co_3(HTTP)_2$ MOF shows metallic character in the stacking direction regardless of the choice of U; however, the intra-layer region shows the most noticeable change with respect to the choice of U. While using U = 0 eV and U = 4 eV results in very small bandgaps in MKΓ and LHA regions, increasing the U parameter to 5.3 eV localizes the 3d states of the Co sites, practically enhancing the extended π–*d* conjugation and intra-layer charge mobility. This effect is manifested in the metallic character in the MKΓ region compared to small bandgaps observed using smaller U parameters. Nevertheless, the observed intra-layer bandgaps in the parent $Co_3(HTTP)_2$ MOF with smaller U parameters are minimal, which confirms the potential of this 2D MOF for band engineering through external stimuli.

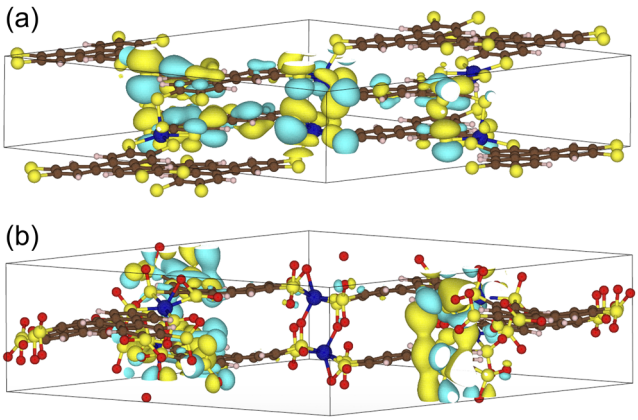

FIG. 6. Calculated charge density isosurfaces of the highest occupied crystal orbitals of the (a) parent and (b) oxygenated $Co_3(HTTP)_2$ systems plotted using VESTA.[68]

TABLE I. Calculated bandgap openings (in meV) subject to three different U parameter values with direct (D) and indirect (I) bandgap openings characterized for each system.

2D MOFs	$Intra_{MK\Gamma}$	$Intra_{LHA}$	$Inter_{\Gamma A}$
Parent $Co_3(HTTP)_2$			
U = 5.3 eV	Metallic	12 (I)	Metallic
U = 4.0 eV	31 (D)	13 (I)	Metallic
U = 0.0 eV	13 (I)	30 (I)	Metallic
Oxygenated $Co_3(HTTP)_2$			
U = 5.3 eV	251 (D)	123 (D)	124 (D)
U = 4.0 eV	205 (D)	89 (I)	90 (D)
U = 0.0 eV	202 (D)	144 (I)	141 (I)

IV. CONCLUDING REMARKS AND OUTLOOK

In this work, we elucidated the possible chemisorption and physisorption of the electroactive O_2 molecules in a representative 2D layered MOF, namely, $Co_3(HTTP)_2$. We showed that not only open-Co(II) sites but also redox-active HTTP linkers take part in adsorption of electroactive dioxygen by forming strong Co=O and S=O bonds. A dramatic change in the layered architecture and charge mobility of $Co_3(HTTP)_2$ was observed after inserting O_2 molecules. Our detailed electronic structure analyses showed that the conductive behavior of the MOF switches from metallic to direct semiconducting upon chemisorption of O_2. In fact, the anisotropic conductive nature of the dry system changes to isotropic as displayed by the intra- and inter-layer bandgap openings at the Fermi level. This drastic change is the direct result of abundance of adsorption sites for O_2 and weak van der Waals interactions between

layers, which allow accommodation of guest molecules in the interlayer space. Generalization of this effect to other 2D MOFs is not a straightforward task, and it needs to be investigated for each structure individually due to differences in the nature of open-metal sites and organic linkers and the degree of deformation of the layers. An example in this work was $Co_3(HHTP)_2$, **2D-Co** in Fig. 2, where oxo functional groups have no tendency for adsorbing oxygen; hence, the structural and electronic changes are expected to be less dramatic compared to the $Co_3(HTTP)_2$ case. In this study, we showed that the formation of S=O and Co=O bonds upon adsorption of the electroactive O_2 molecules creates polaron state localization in the fully oxidized system. The nature and role of the formed polaron states in electrical conductivity can be better analyzed by gauging electron–phonon couplings. With the aim of clarifying this topic, studies on the reorganization energy and charge transfer are currently underway in our group. We believe that the rich host–guest chemistry in 2D conductive MOFs can unveil a new host of applications for these materials, for example, in electronics by tuning their electrical conductivity or in selective adsorptive separation of strategic gaseous mixtures and/or heterogeneous catalysis by tuning their chemical reactivity.

SUPPLEMENTARY MATERIAL

See the supplementary material for the benchmark of the computed band structures and pDOSs with different numbers of *k*-points and Hubbard U parameters, and crystal structures of all studied materials.

ACKNOWLEDGMENTS

This work was supported by the start-up fund from the NJIT and used the Extreme Science and Engineering Discovery Environment (XSEDE), which was supported by NSF Grant Nos. CHE200007 and CHE200008. This research was (partially) enabled by the use of computing resources provided by the HPC center at the NJIT.

DATA AVAILABILITY

The data that support the findings of this study are available within the article and its supplementary material.

REFERENCES

[1]T. Qiu, Z. Liang, W. Guo, H. Tabassum, S. Gao, and R. Zou, "Metal–organic framework-based materials for energy conversion and storage," ACS Energy Lett. **5**, 520–532 (2020).
[2]C. C. Hou and Q. Xu, "Metal–organic frameworks for energy," Adv. Energy Mater. **9**, 1801307 (2019).
[3]W. Xia, A. Mahmood, R. Zou, and Q. Xu, "Metal–organic frameworks and their derived nanostructures for electrochemical energy storage and conversion," Energy Environ. Sci. **8**, 1837–1866 (2015).
[4]L. Zhu, X.-Q. Liu, H.-L. Jiang, and L.-B. Sun, "Metal–organic frameworks for heterogeneous basic catalysis," Chem. Rev. **117**, 8129–8176 (2017).
[5]V. Bernales, M. A. Ortuño, D. G. Truhlar, C. J. Cramer, and L. Gagliardi, "Computational design of functionalized metal–organic framework nodes for catalysis," ACS Cent. Sci. **4**, 5–19 (2018).
[6]D. Farrusseng, S. Aguado, and C. Pinel, "Metal–organic frameworks: Opportunities for catalysis," Angew. Chem., Int. Ed. **48**, 7502–7513 (2009).
[7]K. Sumida, D. L. Rogow, J. A. Mason, T. M. McDonald, E. D. Bloch, Z. R. Herm, T.-H. Bae, and J. R. Long, "Carbon dioxide capture in metal–organic frameworks," Chem. Rev. **112**, 724–781 (2012).
[8]Y. He, W. Zhou, G. Qian, and B. Chen, "Methane storage in metal–organic frameworks," Chem. Soc. Rev. **43**, 5657–5678 (2014).
[9]M. Ding, R. W. Flaig, H.-L. Jiang, and O. M. Yaghi, "Carbon capture and conversion using metal–organic frameworks and MOF-based materials," Chem. Soc. Rev. **48**, 2783–2828 (2019).
[10]H. Kim, S. Yang, S. R. Rao, S. Narayanan, E. A. Kapustin, H. Furukawa, A. S. Umans, O. M. Yaghi, and E. N. Wang, "Water harvesting from air with metal-organic frameworks powered by natural sunlight," Science **356**, 430–434 (2017).
[11]W. Xu and O. M. Yaghi, "Metal–organic frameworks for water harvesting from air, anywhere, anytime," ACS Cent. Sci. **6**, 1348–1354 (2020).
[12]M. J. Kalmutzki, C. S. Diercks, and O. M. Yaghi, "Metal–organic frameworks for water harvesting from air," Adv. Mater. **30**, 1704304 (2018).
[13]M. P. Suh, H. J. Park, T. K. Prasad, and D.-W. Lim, "Hydrogen storage in metal–organic frameworks," Chem. Rev. **112**, 782–835 (2012).
[14]J.-R. Li, J. Sculley, and H.-C. Zhou, "Metal–organic frameworks for separations," Chem. Rev. **112**, 869–932 (2012).
[15]J.-H. Dou, L. Sun, Y. Ge, W. Li, C. H. Hendon, J. Li, S. Gul, J. Yano, E. A. Stach, and M. Dincă, "Signature of metallic behavior in the metal–organic frameworks M_3(hexaiminobenzene)$_2$ (M = Ni, Cu)," J. Am. Chem. Soc. **139**, 13608–13611 (2017).
[16]J. Shen, X. He, T. Ke, R. Krishna, J. M. van Baten, R. Chen, Z. Bao, H. Xing, M. Dinca, Z. Zhang, Y. Qiwei, and Q. Ren, "Simultaneous interlayer and intralayer space control in two-dimensional metal–organic frameworks for acetylene/ethylene separation," Nat. Commun. **11**, 6259 (2020).
[17]D. J. Xiao, E. D. Bloch, J. A. Mason, W. L. Queen, M. R. Hudson, N. Planas, J. Borycz, A. L. Dzubak, P. Verma, K. Lee, F. Bonino, V. Crocellà, J. Yano, S. Bordiga, D. G. Truhlar, L. Gagliardi, C. M. Brown, and J. R. Long, "Oxidation of ethane to ethanol by N_2O in a metal–organic framework with coordinatively unsaturated iron(II) sites," Nat. Chem. **6**, 590–595 (2014).
[18]L. Li, R.-B. Lin, R. Krishna, H. Li, S. Xiang, H. Wu, J. Li, W. Zhou, and B. Chen, "Ethane/ethylene separation in a metal-organic framework with iron-peroxo sites," Science **362**, 443–446 (2018).
[19]J. Oktawiec, H. Z. H. Jiang, J. G. Vitillo, D. A. Reed, L. E. Darago, B. A. Trump, V. Bernales, H. Li, K. A. Colwell, H. Furukawa, C. M. Brown, L. Gagliardi, and J. R. Long, Nat. Commun. **11**, 3087 (2020).
[20]A. S. Rosen, M. R. Mian, T. Islamoglu, H. Chen, O. K. Farha, J. M. Notestein, and R. Q. Snurr, "Tuning the redox activity of metal–organic frameworks for enhanced, selective O_2 binding: Design rules and ambient temperature O_2 chemisorption in a cobalt–triazolate framework," J. Am. Chem. Soc. **142**, 4317–4328 (2020).
[21]M. Hmadeh, Z. Lu, Z. Liu, F. Gándara, H. Furukawa, S. Wan, V. Augustyn, R. Chang, L. Liao, F. Zhou, E. Perre, V. Ozolins, K. Suenaga, X. Duan, B. Dunn, Y. Yamamto, O. Terasaki, and O. M. Yaghi, "New porous crystals of extended metal-catecholates," Chem. Mater. **24**, 3511–3513 (2012).
[22]X. Huang, P. Sheng, Z. Tu, F. Zhang, J. Wang, H. Geng, Y. Zou, C.-A. Di, Y. Yi, Y. Sun, and D. Zhu, "Two-dimensional π–d conjugated coordination polymer with extremely high electrical conductivity and ambipolar transport behavior," Nat. Commun. **6**, 7408 (2015).
[23]L. Sun, M. G. Campbell, and M. Dincă, "Electrically conductive porous metal–organic frameworks," Angew. Chem., Int. Ed. **55**, 3566–3579 (2016).
[24]A. J. Clough, J. M. Skelton, C. A. Downes, A. A. de la Rosa, J. W. Yoo, A. Walsh, B. C. Melot, and S. C. Marinescu, "Metallic conductivity in a two-dimensional cobalt dithiolene metal–organic framework," J. Am. Chem. Soc. **139**, 10863–10867 (2017).
[25]L. S. Xie, G. Skorupskii, and M. Dincă, "Electrically conductive metal–organic frameworks," Chem. Rev. **120**, 8536–8580 (2020).
[26]M. R. Momeni, Z. Zhang, and F. A. Shakib, "Deterministic role of structural flexibility on catalytic activity of conductive 2d layered metal–organic frameworks," Chem. Commun. **57**, 315–318 (2021).

[27]Y. Shi, M. R. Momeni, Y.-J. Chen, Z. Zhang, and F. A. Shakib, "Water-induced structural transformations in flexible two-dimensional layered conductive metal–organic frameworks," Chem. Mater. **32**, 9664–9674 (2020).
[28]M. R. Momeni, Z. Zhang, D. Dell'Angelo, and F. A. Shakib, "Gauging van der Waals interactions in aqueous solutions of 2D MOFs: When water likes organic linkers more than open-metal sites," Phys. Chem. Chem. Phys. **23**, 3135–3143 (2021).
[29]X.-F. Lu, P.-Q. Liao, J.-W. Wang, J.-X. Wu, X.-W. Chen, C.-T. He, J.-P. Zhang, G.-R. Li, and X.-M. Chen, "An alkaline-stable, metal hydroxide mimicking metal–organic framework for efficient electrocatalytic oxygen evolution," J. Am. Chem. Soc. **138**, 8336–8339 (2016).
[30]J. Hutter, M. Iannuzzi, F. Schiffmann, and J. VandeVondele, "cp2k: Atomistic simulations of condensed matter systems," WIREs Comput. Mol. Sci. **4**, 15–25 (2014).
[31]J. P. Perdew, K. Burke, and M. Ernzerhoff, "Erratum: Generalized gradient approximation made simple," Phys. Rev. Lett. **78**, 1396 (1996).
[32]S. Grimme, J. Antony, S. Ehrlich, and H. Krieg, "A consistent and accurate *ab initio* parametrization of density functional dispersion correction (DFT-D) for the 94 elements H-Pu," J. Chem. Phys. **132**, 154104 (2010).
[33]S. Goedecker, M. Teter, and J. Hutter, "Separable dual-space Gaussian pseudopotentials," Phys. Rev. B **54**, 1703–1710 (1996).
[34]A. S. Rosen, J. M. Notestein, and R. Q. Snurr, "Comparing GGA, GGA+*U*, and meta-GGA functionals for redox-dependent binding at open metal sites in metal–organic frameworks," J. Chem. Phys. **152**, 224101 (2020).
[35]F. Crasto de Lima, G. J. Ferreira, and R. H. Miwa, "Layertronic control of topological states in multilayer metal-organic frameworks," J. Chem. Phys. **150**, 234701 (2019).
[36]Z. Li, A. W. Peters, V. Bernales, M. A. Ortuño, N. M. Schweitzer, M. R. DeStefano, L. C. Gallington, A. E. Platero-Prats, K. W. Chapman, C. J. Cramer, L. Gagliardi, J. T. Hupp, and O. K. Farha, "Metal–organic framework supported cobalt catalysts for the oxidative dehydrogenation of propane at low temperature," ACS Cent. Sci. **3**, 31–38 (2017).
[37]M. A. Ortuño, V. Bernales, L. Gagliardi, and C. J. Cramer, "Computational study of first-row transition metals supported on MOF NU-1000 for catalytic acceptorless alcohol dehydrogenation," J. Phys. Chem. C **120**, 24697–24705 (2016).
[38]D. R. Pahls, M. A. Ortuño, P. H. Winegar, C. J. Cramer, and L. Gagliardi, "Computational screening of bimetal-functionalized Zr_6O_8 MOF nodes for methane C–H bond activation," Inorg. Chem. **56**, 8739–8743 (2017).
[39]Y. Zhao and D. G. Truhlar, "A new local density functional for main-group thermochemistry, transition metal bonding, thermochemical kinetics, and noncovalent interactions," J. Chem. Phys. **125**, 194101 (2006).
[40]F. Weigend, "Accurate Coulomb-fitting basis sets for H to Rn," Phys. Chem. Chem. Phys. **8**, 1057–1065 (2006).
[41]F. Weigend and R. Ahlrichs, "Balanced basis sets of split valence, triple zeta valence and quadruple zeta valence quality for H to Rn: Design and assessment of accuracy," Phys. Chem. Chem. Phys. **7**, 3297–3305 (2005).
[42]C. J. Cramer, *Essentials of Computational Chemistry: Theories and Models*, 2nd ed. (John Wiley & Sons, Chichester, 2004).
[43]Y. Zhao and D. G. Truhlar, "The M06 suite of density functionals for main group thermochemistry, thermochemical kinetics, noncovalent interactions, excited states, and transition elements: Two new functionals and systematic testing of four M06-class functionals and 12 other functionals," Theor. Chem. Acc. **120**, 215–241 (2008).
[44]Y. Zhao and D. G. Truhlar, "Density functionals with broad applicability in chemistry," Acc. Chem. Res. **41**, 157–167 (2008).
[45]M. J. Frisch, G. W. Trucks, H. B. Schlegel, G. E. Scuseria, M. A. Robb, J. R. Cheeseman, G. Scalmani, V. Barone, B. Mennucci, G. A. Petersson, H. Nakatsuji, M. Caricato, X. Li, H. P. Hratchian, A. F. Izmaylov, J. Bloino, G. Zheng, J. L. Sonnenberg, M. Hada, M. Ehara, K. Toyota, R. Fukuda, J. Hasegawa, M. Ishida, T. Nakajima, Y. Honda, O. Kitao, H. Nakai, T. Vreven, J. A. Montgomery, Jr., J. E. Peralta, F. Ogliaro, M. Bearpark, J. J. Heyd, E. Brothers, K. N. Kudin, V. N. Staroverov, R. Kobayashi, J. Normand, K. Raghavachari, A. Rendell, J. C. Burant, S. S. Iyengar, J. Tomasi, M. Cossi, N. Rega, J. M. Millam, M. Klene, J. E. Knox, J. B. Cross, V. Bakken, C. Adamo, J. Jaramillo, R. Gomperts, R. E. Stratmann, O. Yazyev, A. J. Austin, R. Cammi, C. Pomelli, J. W. Ochterski, R. L. Martin, K. Morokuma, V. G. Zakrzewski, G. A. Voth, P. Salvador, J. J. Dannenberg, S. Dapprich, A. D. Daniels, O. Farkas, J. B. Foresman, J. V. Ortiz, J. Cioslowski, and D. J. Fox, GAUSSIAN 16, Revision A.03, Gaussian, Inc., Wallingford, CT, 2016.
[46]G. Kresse and J. Hafner, "*Ab initio* molecular dynamics for liquid metals," Phys. Rev. B **47**, 558–561 (1993).
[47]G. Kresse and J. Hafner, "*Ab initio* molecular-dynamics simulation of the liquid-metal–amorphous-semiconductor transition in germanium," Phys. Rev. B **49**, 14251–14269 (1994).
[48]G. Kresse and J. Furthmüller, "Efficiency of ab-initio total energy calculations for metals and semiconductors using a plane-wave basis set," Comput. Mater. Sci. **6**, 15–50 (1996).
[49]G. Kresse and J. Furthmüller, "Efficient iterative schemes for *ab initio* total-energy calculations using a plane-wave basis set," Phys. Rev. B **54**, 11169–11186 (1996).
[50]V. I. Anisimov, J. Zaanen, and O. K. Andersen, "Band theory and Mott insulators: Hubbard *U* instead of Stoner *I*," Phys. Rev. B **44**, 943–954 (1991).
[51]V. I. Anisimov, F. Aryasetiawan, and A. I. Lichtenstein, "First-principles calculations of the electronic structure and spectra of strongly correlated systems: The LDA+*U* method," Theor. Chem. Acc. **9**, 767–808 (1997).
[52]B. Himmetoglu, A. Floris, S. de Gironcoli, and M. Cococcioni, "Hubbard-corrected DFT energy functionals: The LDA+U description of correlated systems," Int. J. Quantum Chem. **114**, 14–49 (2014).
[53]G. W. Mann, K. Lee, M. Cococcioni, B. Smit, and J. B. Neaton, "First-principles Hubbard *U* approach for small molecule binding in metal-organic frameworks," J. Chem. Phys. **144**, 174104 (2016).
[54]P. E. Blöchl, "Projector augmented-wave method," Phys. Rev. B **50**, 17953–17979 (1994).
[55]G. Kresse and D. Joubert, "From ultrasoft pseudopotentials to the projector augmented-wave method," Phys. Rev. B **59**, 1758–1775 (1999).
[56]D. Sheberla, L. Sun, M. A. Blood-Forsythe, S. Er, C. R. Wade, C. K. Brozek, A. Aspuru-Guzik, and M. Dincă, "High electrical conductivity in Ni_3(2,3,6,7,10,11-hexaiminotriphenylene)$_2$, a semiconducting metal–organic graphene analogue," J. Am. Chem. Soc. **136**, 8859–8862 (2014).
[57]E. M. Miner, S. Gul, N. D. Ricke, E. Pastor, J. Yano, V. K. Yachandra, T. Van Voorhis, and M. Dincă, "Mechanistic evidence for ligand-centered electrocatalytic oxygen reduction with the conductive MOF Ni_3(hexaiminotriphenylene)$_2$," ACS Catal. **7**, 7726–7731 (2017).
[58]E. Miner, T. Fukushima, D. Sheberla *et al.*, "Electrochemical oxygen reduction catalysed by Ni_3(hexaiminotriphenylene)$_2$," Nat. Commun. **7**, 10942 (2016).
[59]Y. Lian, W. Yang, C. Zhang, H. Sun, Z. Deng, W. Xu, L. Song, Z. Ouyang, Z. Wang, J. Guo, and Y. Peng, "Unpaired 3d electrons on atomically dispersed cobalt centres in coordination polymers regulate both oxygen reduction reaction (ORR) activity and selectivity for use in zinc–air batteries," Angew. Chem., Int. Ed. **59**, 286–294 (2020).
[60]J. Park, Z. Chen, R. A. Flores, G. Wallnerström, A. Kulkarni, J. K. Nørskov, T. F. Jaramillo, and Z. Bao, "Two-dimensional conductive Ni-HAB as a catalyst for the electrochemical oxygen reduction reaction," ACS Appl. Mater. Interfaces **12**, 39074–39081 (2020).
[61]S. S. Park, E. R. Hontz, L. Sun, C. H. Hendon, A. Walsh, T. Van Voorhis, and M. Dincă, "Cation-dependent intrinsic electrical conductivity in isostructural tetrathiafulvalene-based microporous metal–organic frameworks," J. Am. Chem. Soc. **137**, 1774–1777 (2015).
[62]Y. Kobayashi, B. Jacobs, M. D. Allendorf, and J. R. Long, "Conductivity, doping, and redox chemistry of a microporous dithiolene-based metal–organic framework," Chem. Mater. **22**, 4120–4122 (2010).
[63]J. Cui and Z. Xu, "Conductivity, doping, and redox chemistry of a microporous dithiolene-based metal–organic framework," Chem. Commun. **50**, 3986–3988 (2014).
[64]D. Y. Lee, E.-K. Kim, N. K. Shrestha, D. W. Boukhvalov, J. K. Lee, and S.-H. Han, "Charge transfer-induced molecular hole doping into thin film of metal–organic frameworks," ACS Appl. Mater. Interfaces **7**, 18501–18507 (2015).

[65]Y. Jiang, I. Oh, S. H. Joo, O. Buyukcakir, X. Chen, S. H. Lee, M. Huang, W. K. Seong, S. K. Kwak, J.-W. Yoo, and R. S. Ruoff, "Partial oxidation-induced electrical conductivity and paramagnetism in a Ni(II) tetraaza[14]annulene-linked metal organic framework," J. Am. Chem. Soc. **141**, 16884–16893 (2019).
[66]M. E. Foster, K. Sohlberg, C. D. Spataru, and M. D. Allendorf, "Proposed modification of the graphene analogue $Ni_3(HITP)_2$ to yield a semiconducting material," J. Phys. Chem. C **120**, 15001–15008 (2016).
[67]M. E. Foster, K. Sohlberg, M. D. Allendorf, and A. A. Talin, "Unraveling the semiconducting/metallic discrepancy in $Ni_3(HITP)_2$," J. Phys. Chem. Lett. **9**, 481–486 (2018).
[68]K. Momma and F. Izumi, J. Appl. Crystallogr. **44**, 1272–1276 (2011).
[69]P. Verma and D. G. Truhlar, "HLE17: An improved local exchange–correlation functional for computing semiconductor band gaps and molecular excitation energies," J. Phys. Chem. C **121**, 7144–7154 (2017).
[70]I. Choudhuri and D. G. Truhlar, "HLE17: An efficient way to predict band gaps of complex materials," J. Phys. Chem. C **123**, 17416–17424 (2019).